Special issue article for *Rising Stars 2022 in Polymer Journal*: Accepted

Viscoelastic Properties of Comb-Shaped Ring Polystyrenes

Yuya Doi,[*,1,2] Jinya Kitamura,[1] Takashi Uneyama,[1] Yuichi Masubuchi,[1] Atsushi Takano,[*,2] Yoshiaki Takahashi[3] and Yushu Matsushita[2,4]

[1]*Department of Materials Physics and* [2]*Department of Molecular and Macromolecular Chemistry, Nagoya University, Nagoya 4648603, Japan*

[3]*Institite of Materials Chemistry and Engineering, Kyushu University, Kasuga, Fukuoka 8168580, Japan*

[4]*Toyota Physical and Chemical Research Institute, Nagakute, Aichi 4801192, Japan*

*To whom correspondence should be addressed:

ydoi@mp.pse.nagoya-u.ac.jp (YD) and atakano@chembio.nagoya-u.ac.jp (AT)

ABSTRACT

In this study, we examined the viscoelastic properties of a series of comb-shaped ring (RC) polystyrene samples with different branch chain length, i.e., the molecular weight of the ring backbone M_{bb} ($\simeq 4M_e$ where M_e is the entanglement molecular weight) and branch chains M_{br} ($\simeq M_e$, $2M_e$, and $4M_e$). Even for the RC sample with the shortest branch chains, a plateau region of the dynamic modulus $G^*(\omega)$ was observed in the middle angular frequency ω region, suggesting that intermolecular branch chain entanglement occurs. In the ω region between the plateau and terminal region, $G^*(\omega)$ with a weaker ω dependence than the terminal relaxation was observed. This behavior was more pronounced for the RC samples with shorter branch chains and also for the corresponding linear comb (LC) samples than the RC ones. Molecular weight dependence of zero-shear viscosity η_0 and steady-state recoverable compliance J_e^o of the RC and LC samples was evaluated, and the effect of different molecular structures (i.e., ring or linear) of the backbones on the terminal relaxation behavior was discussed. Moreover, the $G^*(\omega)$ data were analyzed with two models: the comb-Rouse model in which the structure of the RC/LC molecules is taken into account by graph theory, and the Milner-McLeish model for entangled star-shaped polymers. The former model was able to qualitatively describe the terminal relaxation behavior of $G^*(\omega)$ at low ω, but failed to reproduce the plateau in the middle ω range. Conversely, the latter model described the entanglement plateau in the middle ω range, but the difference in the terminal relaxation regime between the RC/LC samples seen in the data and the comb-Rouse model was disappeared.

INTRODUCTION

The molecular architecture of polymers is known to strongly influence various physical properties of polymers, such as viscoelasticity. Elucidation of the correlation between molecular structure and dynamics of polymers is one of the important issues in polymer science. Many studies have been conducted on the dynamics of linear and branched polymers,[1-5] and their properties are well-understood by tube models that assume entangled polymers. Ring polymers, which do not have chain ends, exhibit significantly different dynamics from linear and branched polymers having chain ends.[6-10] Specifically, while linear/branched polymers with sufficiently high molecular weights exhibit a wide plateau region in relaxation modulus due to intermolecular entanglement, ring polymers exhibit a power-law type decay of the modulus,[8,10] suggesting that the global dynamics of the ring chain is considerably different from that of entangled linear/branched polymers. Several molecular models have been proposed to describe the dynamics of ring polymers,[11-12] but they are still not fully understood.

Tadpole-shaped polymers where a single linear chain is connected to a ring exhibit a characteristic viscoelastic property.[10,13-14] That is, the linear chain part of the tadpole polymer spontaneously penetrates into the ring part of another molecule, resulting in significantly slower global relaxation than the individual ring polymer. If the number of branch linear chains connected to a ring is increased, it is expected to show different molecular dynamics from that of the tadpole polymers as well as of the ring ones. These kinds of molecules are called comb-shaped ring (RC) polymers or cyclic graft polymers. Their synthesis and characterization in dilute solution have been mainly reported,[15-18] but to the best of the authors' knowledge, there are no examples of experimental studies that have evaluated viscoelasticity using systematic RC samples. When many branch chains are present in RC molecules, it is expected that the contribution of intermolecular interactions of the branch chains becomes larger than those between the linear and ring parts (i.e., branch and backbone in this case) observed in tadpole polymers. From the viewpoint of fundamental polymer science, it is meaningful to understand the viscoelastic properties of a series of RC polymers.

In examining the dynamics of RC polymers, it is important to understand the dynamics of conventional comb-shaped linear (LC) polymers, which have already been studied well.[19-25] A hierarchical relaxation model has been proposed for the dynamics of entangled LC polymers, where both the branch and backbone chains have molecular weights higher than the entanglement molecular weight M_e, in which the outer branch chains relax first, followed by the inner backbone.[4,26] Roovers and Graessley[19] pioneeringly synthesized two series of LC

polystyrene (PS) samples, which have two different backbone lengths and systematically varied branch lengths, and investigated their viscoelastic properties. They discussed the molecular dynamics of the LC polymers by estimating the molecular weight dependence of zero-shear viscosity η_0 and steady-state recoverable compliance J_e^o. Daniels et al.[20] investigated the viscoelastic properties of a series of well-entangled LC polybutadiene (PB) samples, with variously different molecular weights of the branch and backbone chains. They found out that the behavior can be described by a combination of the relaxation model of entangled star-shaped polymers[27] (for branch chains) and the modified reptation model of linear polymers (for backbone chains).

Based on the above background, in this study we experimentally investigate the viscoelastic properties of a series of RC samples with different branch chain lengths by comparing with the corresponding LC ones, and evaluate the effect of the difference in molecular structure (i.e., linear or ring) of the backbone on the viscoelasticity of comb-shaped polymers. Several viscoelastic parameters such as η_0 and J_e^o of the RC and LC samples are estimated, and their molecular weight dependence is discussed. In addition, the data obtained are analyzed by two models, i.e., the Rouse-Ham model,[28-29] which explicitly introduces the effect of molecular structure based on graph theory[30-31] (hereafter, this model is referred to as "comb-Rouse model"), and the Milner-McLeish model,[27] which describes the relaxation of entangled star-shaped polymers, and the molecular dynamics of the RC molecules is discussed.

EXPERIMENTAL

The synthesis, purification, and characterization of a series of LC and RC polystyrene (PS) samples as well as their backbones (Lbb and Rbb) used in this study were reported previously.[17] The molecular characteristics, i.e., total weight-average absolute molecular weight $M_{w,total}$, molecular weight distribution M_w/M_n, molecular weight of one branch chain $M_{w,br}$, average number of branch chains f (= $M_{w,total} - M_{w,bb}$)/$M_{w,br}$, where $M_{w,bb}$ is the molecular weight of backbones, and volume fraction of branch chains in the molecules Φ_{br} (= fM_{br}/M_{total}), for the LC and RC samples together with their backbones are summarized in Table 1. Details of the characterization methods are described elsewhere.[17] Here, the number in the sample code for the backbone samples denotes M_{bb} in kg/mol (with one significant digit), while that for the LC and RC samples represents M_{br}. The RC-80* sample, which has the exactly same M_{br} to the corresponding LC-80, was newly prepared by the same method in the previous report,[17] and used for the rheological measurements in this study. The entanglement molecular weight M_e of PS is 18.0 kg/mol,[1] and $M_{w,bb}$ is ca. 4 times higher than M_e, while $M_{w,br}$ is roughly 1, 2 and 4

times higher than M_e for the LC-20/RC-20, LC-40/RC-40 and LC-80/RC-80* samples, respectively.

Table 1. Molecular characteristics of a series of LC and RC samples and their backbones

Samples	$M_{w,total}$ [a]	M_w/M_n [b]	$M_{w,br}$ [a]	f [c]	Φ_{br} [d]
	kg/mol	-	kg/mol	-	-
Lbb-70	70.9	1.01	-	-	-
Rbb-70	70.5	1.01	-	-	-
LC-20	491	1.02	20.2	21	0.86
RC-20	434	1.03	19.2	19	0.84
LC-40	1070	1.05	41.5	24	0.93
RC-40	929	1.04	41.5	21	0.92
LC-80	1630	1.08	75.9	21	0.96
RC-80*	1100	1.14	75.9	14	0.94

Estimated from (a) SEC-MALS and (b) SEC with PS standards. Calculated from (c) $f = (M_{w,total} - M_{w,bb})/M_{w,br}$, where $M_{w,bb}$ is the molecular weight of backbones, and (d) $\Phi_{br} = fM_{w,br}/M_{w,total}$.

Dynamic viscoelasticity of the RC and LC samples was measured by an ARES-G2 rheometer (TA-Instruments) with 8 mm diameter and 0.1 rad angle cone and plate geometry. Measurements were performed in a temperature range of 120~220 °C (i.e., the highest temperature was depending on the sample) under nitrogen atmosphere with angular frequency ω ranging from 10^{-1}~10^{2} rad/s under linear strain (≤ 5%). Disk-shaped samples for the measurements were prepared by thermal annealing as reported previously.[13] After the viscoelastic measurements, it was confirmed from size-exclusion chromatography with multi-angle light scattering detector (SEC-MALS) measurements that no thermal degradation of the RC and LC samples occurred.

RESULTS AND DISCUSSION

Linear viscoelastic data of RC samples

Figure 1 shows the master curves of the dynamic modulus $G^*(\omega)$ (= $G' + iG''$, where G' and G'' are storage and loss moduli, respectively, and i is the imaginary unit) and tan δ (= G''/G') against ω for the series of RC and LC samples as well as their backbones. By applying the time-temperature superposition, the data are reduced to the reference temperature $T_r = T_g + 60$ K, where T_g is the glass transition temperature of the samples. That is, the data at each temperature

was first shifted horizontally by a shift factor a_T so that the data at any given temperature (e.g., 160 °C) was used as a reference and tan δ at the other temperatures overlapped. At this time, G' and G'' were also vertically shifted to reflect changes in density and temperature as $b_T = \rho(T_r)T_r/\rho(T)T$, where $\rho(T)$ is the density of PS at temperature T, known as $\rho(T) = 1.2503 - 6.50 \times 10^{-4}\ T$ (ρ in g cm^{-1} and T in K).[32] T_r was then corrected so that the $T - T_r$ dependence of a_T for each sample overlapped with that of linear PS with high molecular weight, using the WLF relationship,[1] $\log a_T = C_1(T - T_r)/(C_2 + T - T_r)$ with $C_1 = 6.3$ and $C_2 = 110$ K.[13,33] Figure 2 shows the $T - T_r$ dependence of a_T for the RC and LC samples, in which a_T of the RC and LC samples can be described well with the single WLF curve.

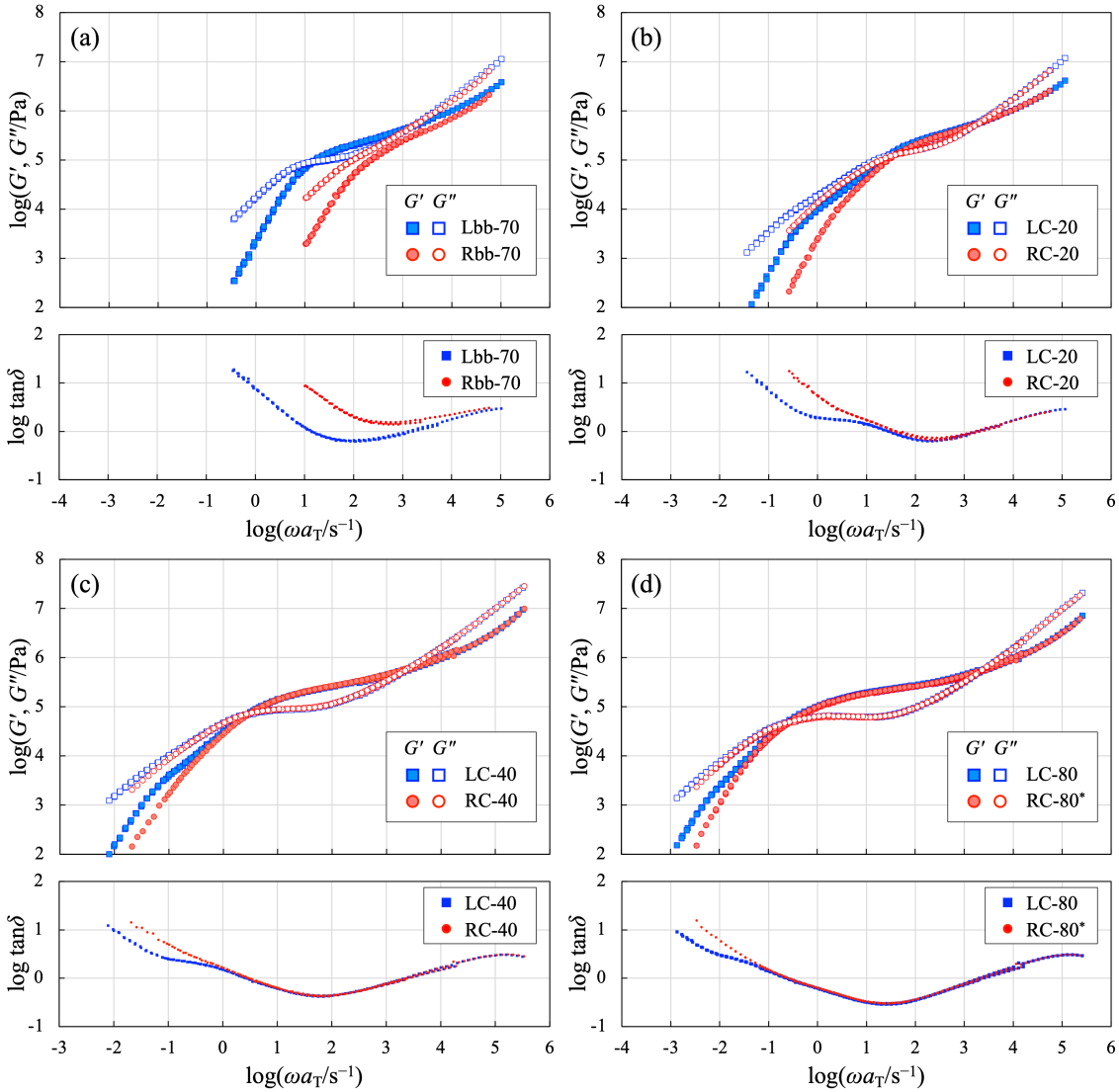

Figure 1. Master curves of G', G'' (top) and tan δ (bottom) for (a) Rbb-70, (b) RC-20, (c) RC-40 and (d) RC-80*, compared with those for the corresponding linear counterparts, reduced at $T_r = T_g + 60$ K.

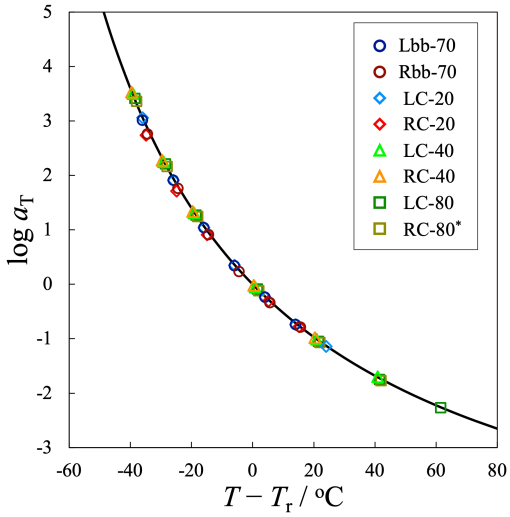

Figure 2. Temperature dependence of log a_T for a series of RC and LC samples as well as their backbones reduced at $T_r = T_g + 60$ K. The solid curve indicates the WLF relationship for linear PS samples as log $a_T = C_1(T - T_r)/(C_2 + T - T_r)$ with $C_1 = 6.3$ and $C_2 = 110$ K.[13]

From Figure 1, the following facts can be found out at first glance. First, in the high ω region of $\omega a_T \gtrsim 10^{3.5}$ s^{-1}, G' and G'' as well as tan δ for the all RC and LC samples are overlapped well, and the overlaid data are shown in Figure S1 in Supplementary Information (SI). This result is associated with the fact that the temperature dependence of a_T shown in Figure 2 can be described by the single WLF curve.

For the backbone samples in Figure 1a, Lbb-70 shows a small entanglement plateau region (i.e., $G' > G''$) in $G^*(\omega)$ at $10^{1.1} \lesssim \omega a_T/\text{s}^{-1} \lesssim 10^{3.2}$, whereas Rbb-70 shows no plateau but reveals an apparent Rouse-like behavior even though its molecular weight is about four times higher than M_e. This result on Rbb-70 is qualitatively similar to that reported for highly-purified ring PS samples.[34]

Regarding the RC and LC samples, an entanglement plateau-like region in $G^*(\omega)$ is observed at $\omega a_T/\text{s}^{-1} = 10^{1.4} \sim 10^{3.2}$ s^{-1} for RC-20 and LC-20 with the shortest M_{br} ($\simeq M_e$), and the region is extended toward lower ω with increasing M_{br}. At sufficiently low ω, a terminal relaxation behavior with $G' \propto \omega^2$ and $G'' \propto \omega^1$ is observed for most of the samples. In the ω region between the plateau and terminal region, there is a region where G' and G'' show a weaker ω dependence than the terminal relaxation, which is also confirmed in tan δ. This behavior is more distinct for the LC samples than for the RC ones, and more evident for the samples with shorter branch chains. Similar trend has been also observed in previous studies of some comb-shaped polymers with linear backbones.[19-22]

When comparing the RC and LC samples with the same branch chain length, their G' and G'' as well as tan δ overlap with each other up to slightly lower ω than the plateau region (at $\omega a_T \gtrsim 10^{1.2}$ s^{-1} for LC-20/RC-20, at $\omega a_T \gtrsim 10^{-0.2}$ s^{-1} for LC-40/RC-40, and at $\omega a_T \gtrsim 10^{-1.2}$ s^{-1} for LC-80/RC-80[*]). Note that the width of the plateau region for LC-20 and RC-20 is slightly different, probably due to the slightly different M_{br} of the samples. For entangled comb-shaped polymers, a hierarchical relaxation mechanism has been proposed, in which the outer entangled branch chains relax first, followed by the inner backbone chains.[4,26] Naively, the agreement in $G^*(\omega)$ of the RC and LC samples with the same M_{br} in the high to middle ω range (from glass transition to plateau region) can be explained by assuming that the branch chain relaxation is dominant in this ω range. In contrast, at the low ω side, the LC samples exhibit slower terminal relaxation behavior than the corresponding RC ones, as can be seen in Figure 1. In other words, in the RC and LC samples examined in this study, the differences in the molecular structure of the backbones are mainly affected at the lower ω region than the entanglement plateau in $G^*(\omega)$.

Several viscoelastic parameters are estimated from $G^*(\omega)$ in Figure 1 in order to discuss the differences between the RC and LC samples. The plateau modulus G_N^o of the samples (except Rbb-70) is determined from the G' value at the minimum tan δ, and the obtained values are summarized in Table 2. Whilst the details are given in SI, the G_N^o values are higher for the RC and LC samples with lower M_{br} (in other words, lower Φ_{br}).

In order to characterize the terminal relaxation behavior of the LC and RC samples, the zero-shear viscosity η_0 and the steady-state recoverable compliance J_e^o, expressed as follows, are estimated:

$$\eta_0 = \lim_{\omega \to 0} \{G''(\omega)/\omega\} \quad (1)$$

and

$$J_e^o = \lim_{\omega \to 0} [\{G'(\omega)/\omega^2\}/[G''(\omega)/\omega]^2] \quad (2)$$

In relation to J_e^o, the complex compliance $J^*(\omega)$ (= $J' - iJ''$, where J' and J'' represent storage and loss compliances, respectively), converted from $G^*(\omega)$ in Figure 1, is shown in Figure S3 in SI. Details on how to actually estimate J_e^o are summarized in SI. The obtained η_0 and J_e^o values for the samples are summarized in Table 2. While η_0 was obtained with high accuracy, J_e^o is shown with error due to the uncertainties involved in its determination.

Table 2. Viscoelastic parameters of the LC and RC samples at $T_r = T_g + 60$ K.

Samples	$10^{-5}G_N^o$	$10^{-5}\eta_0$	$10^5 J_e^o$	$G_N^o J_e^o$
	Pa	Pa s	Pa^{-1}	-
Lbb-70	2.1	0.18	0.73 ± 0.02	1.5
Rbb-70	-	0.015	0.59 ± 0.04	-
LC-20	3.0	0.37	3.9 ± 0.1	11.7
RC-20	2.9	0.14	1.6 ± 0.1	4.7
LC-40	2.4	1.5	5.9 ± 0.3	14.0
RC-40	2.5	0.97	2.7 ± 0.2	6.7
LC-80	2.3	10.1	5.8 ± 0.3	12.9
RC-80*	2.2	7.0	2.7 ± 0.2	5.9

Figures 3 and 4 show the molecular weight dependence of η_0 and J_e^o, respectively, for the RC and LC samples. In Figure 3, η_0 for the RC and LC samples is plotted against M_{br} in double-logarithmic scale, and compared to that for linear PS[34-38] (plotted against M_{total}) and star-shaped PS[39] (plotted against the molecular weight of one arm M_a (= M_{br})) reported elsewhere. For the reference, Figures S4 and S5 in SI show the η_0 and J_e^o data, respectively, plotted against M_{total} for the RC/LC and star PS samples as well as linear PS. If the branch chains in RC and LC molecules are long enough (in other words, if the fraction of the backbone $\Phi_{bb} = 1 - \Phi_{br}$ is small enough), their viscoelastic behavior is expected to be similar to that of star polymers with the same M_{br}. Hence, comparing η_0 of the RC/LC polymers with that of star ones against M_{br} is a good way to discuss the contribution of the backbone in the terminal relaxation of the RC and LC samples.

In Figure 3, linear polymers exhibit $\eta_0 \propto M^1$ below the critical molecular weight M_c ($\simeq 2M_e$), whereas above M_c they show a dependence of η_0 on $M^{3.4}$ due to intermolecular entanglement, as is well-known.[1] (Note that the variation in η_0 data for linear PS at $M < M_c$ is possibly due to the lack of proper correction of T_g.) The η_0 of star polymers is known to increase in an exponential manner independent of the number of arm chains, when plotted against M_a instead of M_{total}.[39,40] As shown in Figure S4 in SI, when plotted against M_{total}, η_0 of the RC and LC samples is evidently lower than that of the linear and star PSs at the same M_{total}. However, as shown in Figure 3, if η_0 is plotted against M_{br}, η_0 of the LC and RC samples in this study is well-above that of linear PSs, and even higher than that of star polymers with the same branch chain length. Since there are only three data points of η_0 for the both LC and RC samples, it is difficult to correctly discuss their molecular weight dependence, but they appear to show a

similar exponential-like viscosity increase as the star polymers. Although η_0 of LC is higher than that of RC at the same M_{br} (as can be seen from Figure 1), the difference in η_0 between the LC and RC samples becomes smaller as M_{br} increases (i.e., $\eta_{0,LC}/\eta_{0,RC}$ = 2.6, 1.6 and 1.4 for LC-20/RC-20, LC-40/RC-40 and LC-80/RC-80*, respectively), and their η_0 appears to asymptotically approach that for star polymers.

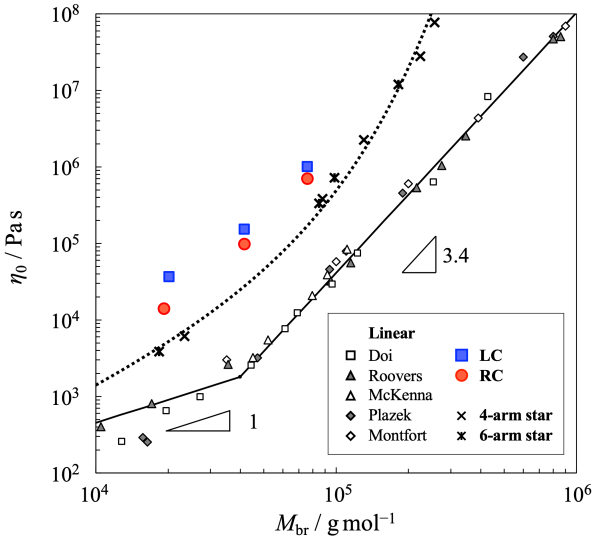

Figure 3. Molecular weight dependence of η_0 for RC and LC samples, compared with linear PSs[34-38] and 4-arm and 6-arm star PSs,[39] reported elsewhere. For the RC/LC and star PS samples, the η_0 data are plotted against M_{br}, while those for linear PSs are against M_{total}. The solid line and the dotted curve indicate the η_0-M dependence for the linear and star PSs, respectively.

In Figure 4, J_e^o for the LC and RC samples is plotted against M_{br}, and compared to that for linear and star PSs, as done in Figure 3. For monodisperse linear polymers, J_e^o is known to increase in proportion to M up to M_c' ($\simeq 5\sim6M_e$), and to remain constant above M_c'.[1] For star polymers, J_e^o continues to proportionally increase to M_{br} even above M_c'.[39] The RC and LC samples measured in this study exhibit considerably higher J_e^o than the star-shaped PS with the same M_{br}. This J_e^o difference between the RC/LC and star polymers is naturally due to the presence or absence of the backbone in molecules, and the associated difference in molecular dynamics. In addition, the RC exhibits a J_e^o value about half as large as the corresponding LC (i.e., $J_{e,RC}^o \simeq 0.4\sim0.5\ J_{e,LC}^o$) irrespective of M_{br}. This J_e^o difference between the RC and LC samples may be due to the difference in the contribution of linear or ring backbone relaxation in the terminal region, if one accepts the idea of the hierarchical relaxation model for comb-shaped polymers.[26] In addition, unlike star polymers, J_e^o values increase from LC-20/RC-20 to LC-40/RC-40, whereas they are apparently saturated from LC-40/RC-40 to LC-80/RC-80*.

Similar molecular weight dependence of J_e^o (i.e., the M_{br}-dependent exponent of J_e^o becomes gradually smaller with increasing M_{br}) is reported for a series of linear comb PSs with equal backbone lengths and different branch chain lengths by Roovers and Graessley.[19]

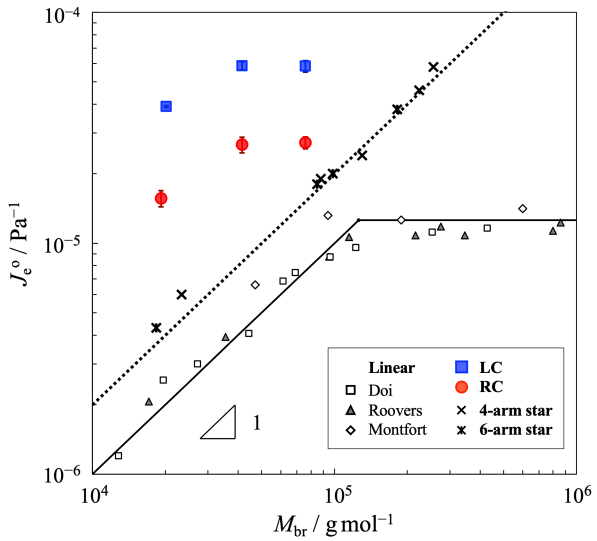

Figure 4. Molecular weight dependence of J_e^o for RC and LC samples compared with linear PS[34,35,38] and 4-arm and 6-arm star PS[39] samples. For the RC/LC and star PS samples, the J_e^o data are plotted against the molecular weight of one branch chain M_{br}, while those for linear PSs are against M_{total}. The solid and dotted lines indicate the J_e^o-M dependence for the linear and star PSs, respectively.

In order to further see the shape of the terminal relaxation for the LC and RC samples, the product of G_N^o and J_e^o, which is a measure of the distribution of terminal relaxation modes, is estimated and summarized in Table 2. $G_N^oJ_e^o$ of the LC samples is higher than that of the RC ones, and much higher than that of well-entangled linear polymers (with $M > M_c$'; $G_N^oJ_e^o = 2.5 \pm 0.5$).[1,3] Moreover, the $G_N^oJ_e^o$ value of the RC samples (as well as the LC ones) is comparable irrespective of the molecular weight of the branch chains. These results suggest that the shape of the terminal relaxation of the RC samples is independent of the branch chain length within the range of the samples examined in this study.

In the following subsections, we analyze the $G^*(\omega)$ data of the RC and LC samples using several molecular models, and further discuss the molecular dynamics of the RC and LC molecules.

Data analysis with comb-Rouse model

The obtained experimental $G^*(\omega)$ data are first analyzed with the discrete spring-bead model,[28] which does not take intermolecular entanglement effects into account. Even for entangled linear

polymers, their dynamics are described based on the motion of spring-bead Rouse chains constrained in a virtual tube,[2] and hence, understanding the Rouse dynamics for the LC and RC polymers is important.

Whilst the details are given in the textbook,[2] the relaxation modulus $G(t)$ of linear polymers based on the spring-bead Rouse model is described as

$$G(t) = (\rho RT/M_{\text{total}}) \sum_{p=1}^{N-1} \exp(-t/\theta_p \tau_{\text{R}}) \quad (3)$$

where ρ is the density of a polymer, R is the gas constant, T is the temperature, M_{total} is the total molecular weight of the polymer, N is the number of total Rouse segments, θ_p is the ratio of the first and pth eigenvalues, λ_1 and λ_p, of the Rouse matrix as

$$\theta_p = \lambda_1/\lambda_p = \sin^2(\pi/2N)/\sin^2(p\pi/2N) \quad (4)$$

τ_{R} is the longest Rouse relaxation time at $p = 1$, and is represented in the high limit of N as

$$\tau_{\text{R}} = \zeta N^2 b^2/6\pi^2 k_{\text{B}} T \quad (5)$$

where ζ is the monomeric friction, b is the segment length, k_{B} is the Boltzmann constant. $G^*(\omega)$ can be actually obtained by Fourier transformation of $G(t)$. For comparison with experimental data for PS, $G^*(\omega)$ of the model is appropriately shifted based on the fact that a linear PS with the molecular weight $M = M_{\text{e}} = 18.0$ kg/mol has a terminal relaxation time $\tau_{\text{R}} = \tau_{\text{e}} = 1.3 \times 10^{-3}$ s at $T_{\text{r}} = T_{\text{g}} + 60$ K.[41]

In contrast to linear homologues, as for ring polymers consisting of N beads, the eigenvalues at even p mode are obtained as double roots in the model. Thus, $G(t)$ of the ring polymers can be written as[42,43]

$$G(t) = (2\rho RT/M_{\text{total}}) \sum_{p:\text{even}}^{N-1} \exp(-t/\theta_p \tau_{\text{R,ring}})$$

with $$\tau_{\text{R,ring}} = \zeta N^2 b^2/24\pi^2 k_{\text{B}} T \quad (6)$$

For polymers having branched architectures, their modulus as well as eigenvalues naturally depend on the molecular structures. In fact, Ham represented branched polymers with arbitral branch points as beads (Rouse segments) connected by springs in matrices.[29] Nitta proposed that the Rouse-Ham matrix can be described by various different types of matrices using graph theory, and reported that the dynamics of polymers with arbitrary branching structure can be described by calculating eigenvalues of the matrices.[30,31]

In this study, we estimated the dynamic modulus from the comb-Rouse model, $G^*_{\text{comb-Rouse}}(\omega)$, for RC and LC molecules with the Rouse segment connections shown in Figure 3 by calculating the eigenvalues of the matrices composed of these connections, following the method by Nitta.[30,31] Note that Nitta treated the systems without any loops in molecular structures in his

reports, but we have confirmed that the calculation on polymers with loops (i.e., Rbb and RC) is also available. Here, the number of beads in one branch chain is n_{br}, the number of backbone beads between adjacent branches is n_{bb}, and the number of a repeating unit is defined as q. For simplicity, branch chains are assumed to be linked to the backbone at equal intervals. In addition, the LC samples are modeled as such that the branch chains are linked to both ends of the backbone, based on the actual molecular structure.[17] The structural parameters for the RC and LC samples used in this study, calculated based on the Rouse segment molecular weight of 850 g/mol for PS,[24,25,44] are summarized in Table 3. The matrix eigenvalues for each sample were calculated using the open-source GNU Octave software (ver. 5.2.0) which utilizes LAPACK for linear algebra calculations. The eigenvalues given were substituted into eq. 3 so as to obtain $G(t)$, resulted in getting $G^*(\omega)$, for the LC and RC samples.

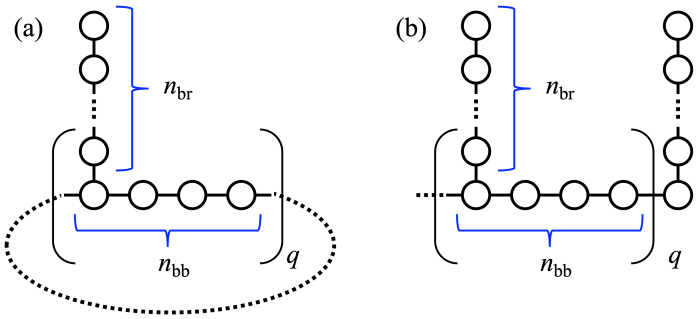

Figure 5. Schematic representation of (a) RC and (b) LC molecules by the connection of beads with the structural parameters n_{br}, n_{bb} and q.

Table 3. Structural parameters in graph theory for a series of LC and RC samples

Samples	n_{bb}	n_{br}	q	n_{total} [a]
Lbb-70	84	0	1	84
Rbb-70	84	0	1	85
LC-20	4	24	20	585
RC-20	4	23	19	513
LC-40	4	49	23	1269
RC-40	4	49	21	1113
LC-80	4	89	20	1950
RC-80*	6	89	14	1330

(a) Calculated from $n_{total} = q(n_{bb} + n_{br})$ for RC and $n_{total} = q(n_{bb} + n_{br}) + (1 + n_{br})$ for LC molecules.

Figure 6 compares the experimental $G^*(\omega)$ data for the series of RC and LC samples with the predictions of the comb-Rouse model (thin curves). The complex modulus of the model is shown as $G^*_{\text{Model-1}} = G^*_{\text{comb-Rouse}} + G^*_{\text{glass}}$, where G^*_{glass} represents the modulus of the glassy mode as $G''_{\text{glass}} = 10^{1.95}\omega$ in accordance with the experimental data. Here, G' of the glassy mode, G'_{glass}, is not considered, because G'_{glass} has little effect in this observation window. A direct comparison of $G^*_{\text{Model-1}}$ between the LC and RC samples is shown in Figure S7 in SI.

Regarding the backbone samples in Figure 6a, it is obvious that the experimental $G^*(\omega)$ of Lbb-70 cannot be described by $G^*_{\text{Model-1}}$ since Lbb-70 shows an entanglement plateau. For Rbb-70, the model describes the data well at high ω with $\omega a_T \gtrsim 10^{2.6}$ s^{-1}, but at lower ω the relaxation of the data is slightly but non-negligibly slower than the model. This result is apparently inconsistent with that for previous highly-purified ring PS samples with similar molecular weights.[34] One possibility might be the presence of a very small amount of linear chain precursor (Lbb-70) in Rbb-70 as an impurity. Another possibility might also be due to some intermolecular interaction between the vinyl group type functional groups (ca. 20 units randomly present in about 700 styrene monomers in the main chain), which serve as branch chain linkage points in the RC sample. Although we do not know the exact reason, we believe that this slight deviation of the Rbb-70 data from the Rouse model has not significantly affect the following discussion on the RC and LC samples.

For the RC-20 and LC-20 samples with short branch chains in Figure 6b, $G^*_{\text{Model-1}}$ does not apparently describe the experimental $G^*(\omega)$ data. Specifically, $G^*_{\text{Model-1}}$ fails to reproduce the plateau region (i.e., $G' > G''$) of the experimental $G^*(\omega)$ seen at $\omega a_T/\text{s}^{-1} = 10^{1.4} \sim 10^{3.2}$ s^{-1} for both RC-20 and LC-20. This result suggests that entanglement between branch chains occurs in the RC-20 and LC-20 samples even though their M_{br} is just close to M_e. On the low ω side, the model shows a considerably faster relaxation than the data, but the shape of $G^*(\omega)$ is similar to each other in between the data and model. That is, at ω region lower than the plateau region in RC-20, the model exhibits relatively simple terminal relaxation behavior, whereas in LC-20, the model shows weaker ω dependence for G' and G'' than the terminal relaxation at $10^{0.7} \lesssim \omega a_T/\text{s}^{-1} \lesssim 10^{2.2}$. From the above, the comb-Rouse model that explicitly takes into account the branching structure of the molecules qualitatively reproduces the terminal relaxation behavior of the RC-20 and LC-20 samples, although some time-scale corrections (e.g., by introducing entanglement effects) are necessary.

For the LC-40/RC-40 and LC-80/RC-80* samples with long branch chains, the $G^*_{\text{model-1}}$ reproduces the experimental data only at $\omega a_T \gtrsim 10^{4.0}$ s^{-1} for G' and at $\omega a_T \gtrsim 10^{2.2}$ s^{-1} for G'', but fails to explain the data covering the other ω range, probably due to entanglement effects between the branch chains. Focusing on $G^*_{\text{Model-1}}$ for the LC and RC molecules with the same branch chain length, the difference in backbone structure is pronounced only on the lower ω side than the power law behavior of $G^*_{\text{Model-1}}$, which is specific to the Rouse model (i.e., $G' \propto G'' \propto \omega^{1/2}$). This trend itself is qualitatively consistent with the experimental $G^*(\omega)$ data for the RC and LC samples. Notably, unlike the hierarchical relaxation model of entangled branched polymers,[26] $G^*_{\text{comb-Rouse}}$ describes the molecular motion without separating that of the backbone and branches. Thus, it is significant that the difference in terminal relaxation behavior between the RC and LC samples could be qualitatively expressed from the comb-Rouse model that reflects the intrinsic molecular structure without using the hierarchical relaxation model.

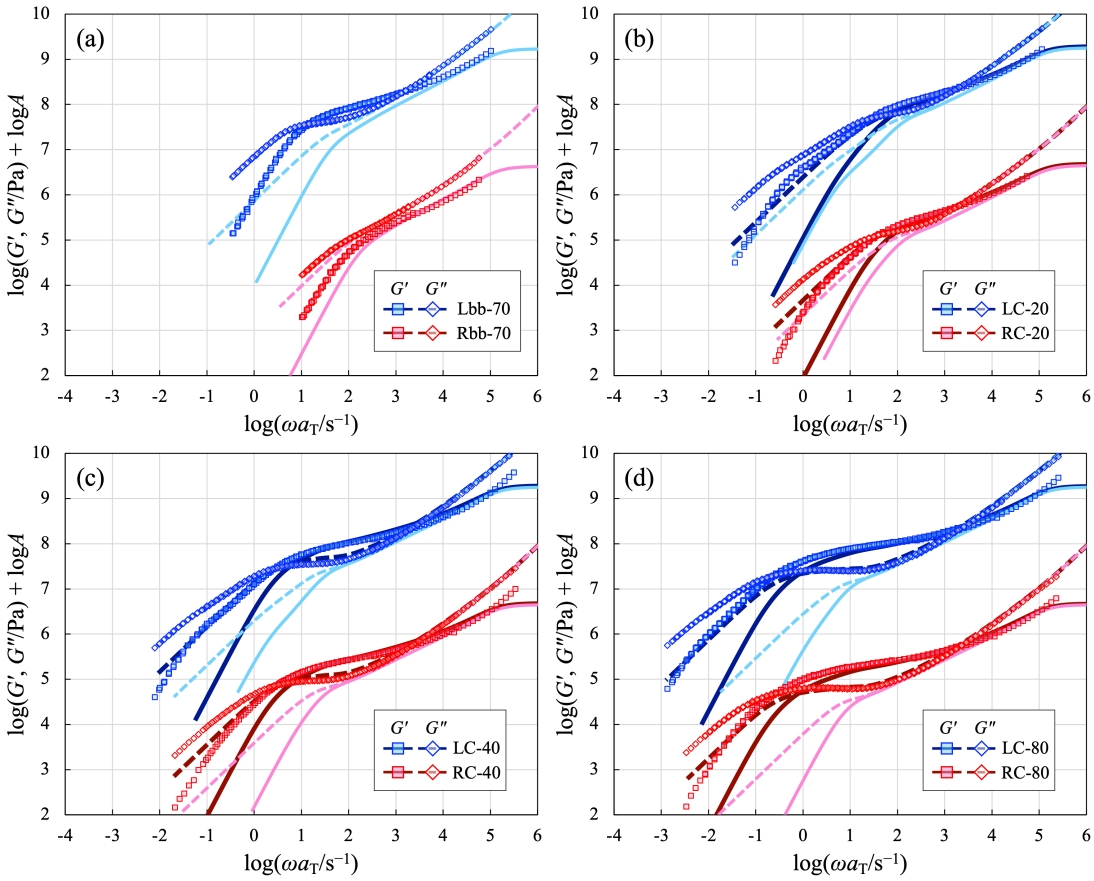

Figure 6. $G^*(\omega)$ for (a) Rbb-70, (b) RC-20, (c) RC-40 and (d) RC-80* compared with those for the corresponding linear counterparts. The data (symbols) are compared with the prediction (curves) of $G^*_{\text{Model-1}} = G^*_{\text{comb-Rouse}} + G^*_{\text{glass}}$ (thin) and $G^*_{\text{Model-2}} = G^*_{\text{MM}} + G^*_{\text{comb-Rouse}} + G^*_{\text{glass}}$ (thick). $G^*(\omega)$ for the Lbb and LC samples are vertically shifted by a factor of $A = 400$.

Data analysis with entanglement polymer model

In the previous subsection, we found out that the comb-Rouse model which takes into account the branching structure explicitly does not adequately express the $G^*(\omega)$ data for the RC and LC samples in this study. Specifically, it was suggested that intermolecular entanglement of branch chains occurs even in the RC-20/LC-20 samples with short branch chains.

Therefore, in this subsection, we attempt to describe the viscoelastic data of the RC and LC samples by assuming that the branch chain entanglement relaxation of the RC and LC samples can be described by the model for entangled star polymers. Here, we applied the Milner-McLeish (MM) model,[27] which considered the dynamics of arm retraction motion with introducing the concept of dynamic tube dilution in star polymers. Specifically, we attempt to describe the experimental data by considering the branch chain entanglement contribution G^*_{MM}, in addition to $G^*_{\text{comb-Rouse}}$ and G^*_{glass} calculated in the previous subsection: $G^*_{\text{Model-2}} = G^*_{\mathrm{MM}} + G^*_{\text{comb-Rouse}} + G^*_{\mathrm{glass}}$. Note that the simple addition of G^*_{MM} and $G^*_{\text{comb-Rouse}}$ is not actually correct (because the dynamics assumed by the two models are not independent), but still this treatment tells us to what extent the viscoelastic data in terminal region can be correctly described. Whilst the details of the MM model are given in the original paper,[27] the parameters, $M_e = 18.0$ kg/mol, $\tau_e = 1.3 \times 10^{-3}$ s, $G_N = 2.1 \times 10^5$ Pa and tube dilution parameter $d = 1$, are used in the present study. The number of branch chain entanglement Z_{br} is estimated as $Z_{br} = M_{w,br}/M_e$. Even using these experimentally determined parameters, quantitative differences between the data and the model are known to exist.[27] In SI, the viscoelasticity data for 4-armed star PSs reported by Graessley and Roovers[39] are fitted by the MM model, and the differences between the model and the data are discussed. In particular, we adopt an additional horizontal shift factor $\log x = -0.4$ for the G^*_{MM} of the LC and RC samples, which is the same value as that required to describe the $G^*(\omega)$ data of the star PSs. As for the tube dilution parameter, we confirmed that the model fits the data better when $d = 1$ rather than $d = 4/3$ for the LC and RC samples.

In Figure 6, $G^*(\omega)$ data (symbols) for the LC and RC samples are compared with $G^*_{\text{Model-2}}$ (thick curves). A direct comparison of $G^*_{\text{Model-2}}$ between the LC and RC samples is shown in Figure S7 in SI. The G^*_{MM} term in the $G^*_{\text{Model-2}}$ is vertically shifted by $\log y = 0.25$ for LC-20/RC-20, 0.20 for LC-40/RC-40, and 0.05 for LC-80/RC-80*, in addition to the common horizontal shift ($\log x = -0.4$), for better agreement with the experimental data. Note that for the LC and RC samples with the same branch chain lengths, the same shift factors are applied since the G^* data in the plateau region are in good agreement with each other. $\log y$ is larger for the LC/RC

samples with shorter branch chains. This result is probably because the contribution of G^*_{MM} in $G^*_{Model\text{-}2}$ is related to Φ_{br} in the LC/RC molecules, as proposed in the hierarchical relaxation model for comb-shaped polymers.[20,22] In fact, we confirmed in Table 1 and Figure S2 in SI that the G_N^o value of the LC and RC samples used in this study becomes higher for lower M_{br} (i.e., lower Φ_{br}).

Figure 6 shows that $G^*_{Model\text{-}2}$ reproduces the $G^*(\omega)$ data well in the high to middle ω range, including the glass transition and part of entanglement plateau, for the all LC and RC samples examined in this study. In contrast, at low ω, $G^*(\omega)$ data are not well-described by $G^*_{Model\text{-}2}$. In fact, the plateau region predicted by $G^*_{Model\text{-}2}$ is slightly but non-negligibly narrower than that of the data, which is clearly different from the results of star polymers as shown in Figure S5 in SI. More importantly, $G^*_{Model\text{-}2}$ for RC-40 and RC-80* is almost perfectly overlapped with that of the corresponding LC samples. This fact means that the model does not correctly present the differences in terminal relaxation behavior between the RC and LC samples, which was observed in the experimental data as well as in $G^*_{Model\text{-}1}$. These results suggest that $G^*_{Model\text{-}2}$ evidently lacks a contribution to reflect the effects of the differences in backbone structure in the RC and LC samples.

As a summary of the model analyses, we clarified that neither the comb-Rouse model nor the MM model can accurately reproduce the viscoelastic data of the RC samples in this study. In fact, to the best of our knowledge, no specific model exists to describe the viscoelastic data of RC polymers (as well as no viscoelastic data of a series of RC polymers exist prior to this study). Thus, as a first step, we believe it is worthwhile to show the fact that the data of the RC samples cannot be reproduced by the above models. As an idea to better describe the experimental results, in the future, we will examine to develop the hierarchical relaxation model to the RC samples.

CONCLUSION

In this study, the viscoelastic properties of systematic RC samples with different branch length (i.e., $M_{bb} \simeq 4M_e$ and $M_{br} \simeq M_e$, $2M_e$, and $4M_e$) were investigated by comparing with the corresponding LC ones. Even the RC-20 and LC-20 samples with shorter branch chains exhibited an entanglement plateau of $G^*(\omega)$ in the middle ω region, and its region is extended with increasing branch chain length in the RC/LC samples. We attribute this region to the contribution of intermolecular entanglement of the branch chains. In the low ω region, all the samples exhibited terminal relaxation behavior. In the ω region between the plateau and

terminal regions, the G' and G'' showed a weaker ω dependence than the terminal relaxation. This behavior was more pronounced for the LCs than the RCs, and also for the samples with shorter branches (i.e., the larger fraction/relaxation contribution of the backbone). η_0 for the RC and LC samples was considerably higher than that of star polymers with the same M_{br}, but the molecular weight dependence of η_0 for the RC and LC samples showed a similar exponential-like dependence for star polymers. Moreover, the ratio of η_0 between the LC and RC samples becomes smaller as M_{br} increases, and their η_0 appears to asymptotically approach that for star polymers. J_e^o of the RC and LC samples first increases and then converged to an apparently constant value with increasing branch chain length. By reflecting the difference in backbone structures, J_e^o of RC was almost half of that of the corresponding LC, irrespective of M_{br}. Moreover, the product $G_N^o J_e^o$ of the RC samples is higher than that of the LC ones, and the $G_N^o J_e^o$ value of the RC (as well as LC) ones is comparable irrespective of the molecular weight of branch chains. These results suggest that the shape of the terminal relaxation of the RC samples is independent of the branch chain length within the range of the samples examined in this study.

The experimental viscoelasticity data obtained were analyzed using $G^*_{comb\text{-}Rouse}$ which reflects the molecular structure explicitly by matrix description using graph theory. $G^*_{comb\text{-}Rouse}$ failed to reproduce the plateau of the G^* data in the medium ω range for all LC and RC samples. At low ω, the model showed considerably faster relaxation than the data, but the shape of G^* exhibited similarity between the model and the data. It is worthwhile that the model was able to qualitatively reproduce the terminal relaxation data in the LC and RC samples, without separating the motion of the branch and backbone chains, unlike the hierarchical relaxation model. We also attempted to describe the G^* data for the LC and RC samples by adding the G^*_{MM}, which was estimated from the Milner-McLeish star polymer entanglement relaxation model, to the $G^*_{comb\text{-}Rouse}$. By introducing G^*_{MM}, the model showed better agreement with the data, but was still incomplete. Specifically, the plateau region in G^* predicted by the model was narrower than the data, and the difference in G^* between the LC and RC samples in the terminal relaxation region on the low ω side disappeared in this model, which was visible in the data and in the $G^*_{comb\text{-}Rouse}$. In the summary of the data analyses, the two models used in this study could not fully describe the data for the RC and LC samples. It is interesting to note, however, that $G^*_{comb\text{-}Rouse}$, which takes the molecular structure into account, was able to describe the differences between the LC and RC samples at the low ω side of $G^*(\omega)$. In the future, we will modify the existing hierarchical relaxation model to better describe the experimental data by appropriately introducing the contribution of slow relaxation of ring backbones.

ACKNOWLEDGEMENTS

The authors acknowledge Prof. H. Watanabe at Kyoto University for his valuable suggestions, especially for the Rouse analysis. The authors thank Dr. J. Roovers for his kind provision of the rheological data for star polystyrenes. This work was supported by JSPS Research Fellowships for Young Scientists (No. 14J03393 for Y.D.) and Grant-in-Aids for Scientific Research (No. 21K14682 for Y.D. and 24350056 for A.T.) This work was partly supported by the Collaborative Research Program of the Institute for Chemical Research, Kyoto University (Grant No. 2015-58), and A.T. is grateful for the support. This work was also supported by the Program for Leading Graduate Schools at Nagoya University entitled "Integrate Graduate Education and Research Program in Green Natural Sciences".

REFERENCES

1. Ferry JD. Viscoelastic properties of polymers. John Wiley and Sons, New York: 1980.
2. Doi M, Edwards SF. The theory of polymer dynamics. Clarendon, Oxford: 1986.
3. Watanabe H. Viscoelasticity and dynamics of entangled polymers. Prog Polym Sci. 1999;24:1253-403.
4. McLeish TCB. Tube theory of entangled polymer dynamics. Adv Phys. 2002;51:1379-527.
5. Graessley WW. Polymeric liquids and network: dynamics and rheology. Garland Science, New York: 2004.
6. Roovers J. Melt properties of ring polystyrenes. Macromolecules. 1985;18:1359-61.
7. Kawaguchi D. Direct observation and mutual diffusion of cyclic polymers. Polym J. 2013;45:783-9.
8. Vlassopoulos D. Molecular topology and rheology: beyond the tube model. Rheol Acta. 2016;55:613-32.
9. Richter D, Goossen S, Wischnewski A. Celebrating Soft Matter's 10th anniversary: topology matters: structure and dynamics or ring polymers. Soft Matter. 2015;11:8535-49.
10. Doi Y. Rheological properties of ring polymers and their derivatives. Nihon Reoroji Gakkaishi (J Soc Rheol Jpn). 2022;50:57-62.
11. Obukhov SP, Rubinstein M, Duke T. Dynamics of a ring polymer in a gel. Phys Rev Lett. 1994;73:1263-6.
12. Ge T, Panyukov S, Rubinstein M. Self-similar conformations and dynamics in entangled melts and solutions of nonconcatenated ring polymers. Macromolecules. 2016;49:708-22.
13. Doi Y, Takano A, Takahashi Y, Matsushita Y. Melt rheology of tadpole-shaped polystyrenes. Macromolecules. 2015;48:8667-74.

14. Doi Y, Takano A, Takahashi Y, Matsushita Y. Melt rheology of tadpole-shaped polystyrenes with different ring sizes. Soft Matter. 2020;16:8720-4.

15. Xia Y, Boydston AJ, Grubbs RH. Synthesis and direct imaging of ultrahigh molecular weight cyclic brush polymers. Angew Chem Int Ed. 2011;50:5882-5.

16. Schappacher M, Deffieux A. Atomic force microscopy imaging and dilute solution properties of cyclic and linear polystyrene combs. J Am Chem Soc. 2008;130:14684-9.

17. Doi Y, Iwasa Y, Watanabe K, Nakamura M, Takano A, Takahashi Y. Synthesis and characterization of comb-shaped ring polystyrenes. Macromolecules. 2016;49:3109-15.

18. Zhang S, Tezuka Y, Zhang Z, Li Na, Zhang W, Zhu L. Recent advances in the construction of cyclic grafted polymers and their potential applications. Polym Chem. 2018;9:677-86.

19. Roovers J, Graessley WW. Melt Rheology of Some Model Comb Polystyrenes. Macromolecules. 1981;14:766-73.

20. Daniels DR, McLeish TCB, Crosby BJ, Young RN, Fernyhough CM. Molecular rheology of comb polymer melts. 1. linear viscoelastic response. Macromolecules. 2001;34:7025-33.

21. Kapnistos M, Vlassopoulos D, Roovers J, Leal LG. Linear rheology of architecturally complex macromolecules: comb polymers with linear backbones. Macromolecules. 2005;38:7852-7862.

22. Inkson NJ, Graham RS, McLeish TCB, Groves DJ, Fernyhough CM. Viscoelasticity of monodisperse comb polymer melts. Macromolecules. 2006;39:4217-27.

23. Kirkwood KM, Leal LG, Vlassopoulos D, Driva P, Hadjichristidis N. Stress relaxation of comb polymers with short branches. Macromolecules. 2009;42:9592-608.

24. Iwawaki H, Inoue T, Nakamura Y. Rheo-optical study on bottlebrush-like polymacromonomer consisting of polystyrene. Macromolecules. 2011;44:5414-9.

25. Iwawaki H, Urakawa O, Inoue T, Nakamura Y. Rheo-optical study on dynamics of bottlebrush-like polymacromonomer consisting of polystyrene. II. Side chain length dependence on dynamical stiffness of main chain. Macromolecules. 2012;45:4801-8.

26. McLeish TCB. Hierarchical relaxation in tube models of branched polymers. Europhys Lett. 1988;6:511-6.

27. Milner ST, McLeish TCB. Parameter-free theory for stress relaxation in star polymer melts. Macromolecules. 1997;30:2159-2166.

28. Rouse PE. A Theory of the linear viscoelastic properties of dilute solutions of coiling polymers. J Chem Phys. 1953;21:1272-80.

29. Ham JS. Viscoelastic theory of branched and cross-linked polymers. J Chem Phys. 1957;26:625-33.

30. Nitta K. A Graph-theoretical approach to statics and dynamics of treelike molecules. J Math Chem. 1999;25:133-43.

31. Nitta K. Graph-theoretical method for Rouse-Ham dynamics. Nihon Reoroji Gakkaishi (J Soc Rheol Jpn). 2002;30:49-54.

32. Zoller P, Walsh D. Standard pressure-volume-temperature data for polymers. Technomic Pub: 1995.

33. Doi Y, Takano A, Takahashi Y, Matsushita Y. Viscoelastic properties of dumbbell-shaped polystyrenes in bulk and solution. Macromolecules. 2020;54:1366-74.

34. Doi Y, Matsubara K, Ohta Y, Nakano T, Kawaguchi D, Takahashi Y, Takano A, Matsushita Y. Melt rheology of ring polystyrenes with ultrahigh purity. Macromolecules. 2015;48:3140-7.

35. Roovers J. Viscoelastic properties of polybutadiene rings. Macromolecules. 1988;21:1517-21.

36. McKenna GB, Hostetter BJ, Hadjichristidis N, Fetters LJ, Plazek DJ. A study of the linear viscoelastic properties of cyclic polystyrenes using creep and recovery measurements. Macromolecules. 1989;22:1834-52.

37. Plazek DJ, O'Rourke VM. Viscoelastic behavior of low molecular weight polystyrene. J Polym Sci Part A-2: Polym Phys. 1971;9:209-43.

38. Montfort JP, Marin G, Monge P. Effects of constraint release on the dynamics of entangled linear polymer melts. Macromolecules. 1984;17:1551-60.

39. Graessley WW, Roovers J. Melt rheology of four-arm and six-arm star polystyrenes. Macromolecules. 1979;12:959-65.

40. Fetters LJ, Kiss AD, Pearson DS, Quack GF, Vitus FJ. Rheological behavior of star-shaped polymers. Macromolecules. 1993;26:647-54.

41. Doi Y, Matsumoto A, Inoue T, Iwamoto T, Takano A, Matsushita Y, Takahashi Y, Watanabe H. Re-examination of terminal relaxation behavior of high-molecular-weight ring polystyrene melts. Rheol Acta. 2017;56:567-81.

42. Watanabe H, Inoue T, Matsumiya Y. Transient conformational change of bead-spring ring chain during creep process. Macromolecules. 2006;39:5419-26.

43. Tsolou GT, Stratikis N, Baig C, Stephanou PS, Marvantzas VG. Melt structure and dynamics of unentangled polyethylene riings: Rouse theory, atomistic molecular dynamics simulation, and comparison with the linear analogues. Macromolecules. 2010;43:10692-713.

44. Inoue T, Okamoto H, Osaki K. Birefringence of amorphous polymers. 1. dynamic measurement on polystyrene. Macromolecules. 1991;24:5670-5.

TOC Graphic

Viscoelastic Properties of Comb-Shaped Ring Polystyrenes

Yuya Doi,[*,1,2] Jinya Kitamura,[1] Takashi Uneyama,[1] Yuichi Masubuchi,[1] Atsushi Takano,[*,2] Yoshiaki Takahashi[3] and Yushu Matsushita[2,4]

[1]*Department of Materials Physics and* [2]*Department of Molecular and Macromolecular Chemistry, Nagoya University, Nagoya 4648603, Japan*

[3]*Institite of Materials Chemistry and Engineering, Kyushu University, Kasuga, Fukuoka 8168580, Japan*

[4]*Toyota Physical and Chemical Research Institute, Nagakute, Aichi 480-1192, Japan*